

Time Crystal Embodies Chimera in Periodically Driven Quantum Spin System

Mahbub Rahaman,^{1,*} Akitada Sakurai,² and Analabha Roy^{1,†}

¹*Department of Physics, The University of Burdwan, Burdwan 713104, India*

²*Quantum Information Science and Technology Unit,*

Okinawa Institute of Science and Technology Graduate University, Onna-son, Okinawa 904-0495, Japan

Chimera states are a captivating occurrence in which a system comprised of multiple interconnected elements exhibits a distinctive combination of synchronized and de-synchronized behavior. The emergence of these states can be attributed to the complex interdependence between quantum entanglement and the delicate balance of interactions among system constituents. The emergence of Discrete Time Crystal (DTC) in typical many-body periodically driven systems occurs when there is a breaking of time translation symmetry. Coexisting coupled DTC and a ferromagnetic dynamically many-body localized (DMBL) phase at distinct regions have been investigated under the controlled spin rotational error of a disorder-free spin-1/2 chain for different types of spin-spin interactions. We contribute a novel approach for the emergence of the DTC-DMBL-Chimera phase, which is robust against external static fields in a periodically driven quantum many-body system.

Keywords: Dynamical Many Body localization, Chimera in a quantum system, Time crystal, Periodic drive.

In classical systems, the coexistence of coupled spontaneous synchronized and de-synchronized dynamics has been known to emerge in the dynamics of coupled systems of identical oscillators. This type of emergent behavior is called a *Chimera State* [1–3]. The idea of chimera has been brought to the quantum regime. For example, the chimera phase can also be realized in quantum many-body systems, and chimera order has been investigated as a quantum phase of matter [4]. However, because non-linearity plays an essential role in their co-existence in classical systems, making the chimera state in closed quantum systems seems challenging since unitary dynamics are linear. Given this point, the quantum version of the chimera phase has been proposed in the semi-classical regimes.

However, it does not reject the possibility of a chimera state even if it is closed quantum system, but one needs to take a different approach to make a system where two different dynamics coexist in one closed system. A new type of chimera state or chimera like state has been proposed and reported in many-body systems. MR: This sentence should be clearer. Please rewrite it. In recent decades, interest has risen in realizing chimeras in magnetic systems. Here, magnetic order and disorder co-exist in systems of interacting quantum spins that can be represented by the quantum Ising model [5]. Recent advancements in this domain involve the formation of a *chimera time crystalline order*, as reported by Sakurai *et al.* [6], where stable chimeras were obtained by the application of disorder in a one-dimensional interacting spin-1/2 chain. A chimera state shows that a stable *Discrete Time Crystal* (DTC) phase can exist even it is surrounded by another dynamical state. DTC is a state of matter that emerges

from the breaking of discrete time translational symmetry [7].

In the original proposal, Sakurai *et al.* considered an Ising type spin-1/2 system and applied Many-Body Localization(MBL) which emerges from disorder introduced in the system. MBL prevents DTC from thermalizing, without which every part of the system would regard the rest of the system as a heat-bath, eventually reaching thermal equilibrium [7–11]. Thereby MBL protects the coexistence of two different phases. In the original proposal, they used the many-body localization (MBL) to prevent thermalization in the DTC phase and to protect coexistence of two different dynamics, and to make MBL they considered the Ising model. Now, it is natural to consider whether a chimera state can exists in the more general cases in which the interactions which do not contribute to the localization but prompt the thermalization. For instance, ~~because of~~ the Heisenberg interaction has off-diagonal elements, ~~because it~~ which allows the magnetization traveling, it seems to break the chimera state.

This paper In this paper we investigate a new chimera comprised of a DTC state in the a disorder-free spin-1/2 chain having the Heisenberg interaction. In our model, instead of the MBL, we consider the Dynamical Many-Body Localization (DMBL) [12–18] via Coherent Destruction of Tunneling (CDT/DL) [19, 20] by applying the external time-periodic driving to prevent the thermalization of DTC and construct the chimera state. To break the discrete time discrete translational symmetry and realize the DTC phase, we consider a periodically driven transverse field that breaks \mathbb{Z}_2 symmetry. We will show that even the influence of the Heisenberg interaction is also suppressed in the chimera state. And we also show the chimera DTC state is robust against the external static and time periodic driving fields. Our work will contribute to the quantum engineering and designing the quantum memory based on the DTC.[8]

We present our work as follows: In section I, we de-

* Primary and corresponding author;
Email: mrahaman@scholar.buruniv.ac.in

† Co-corresponding author;
Email: daneel@utexas.edu

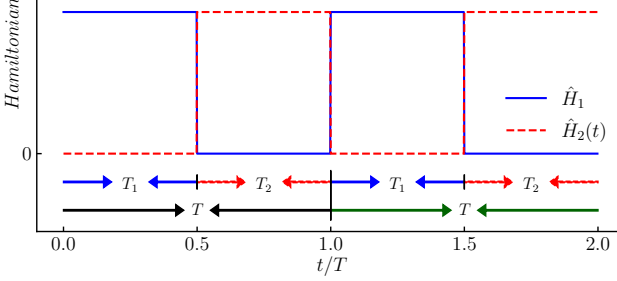


FIG. 1. Pictorial realization of the temporal progression of the Hamiltonian in Eqn 1. The modulating pulses are set in such a way that the spin-flipping Hamiltonian \hat{H}_1 , depicted as Eqn 2, acts during the T_1 -cycle (blue curve), and the harmonic drive as well as the interactions, depicted as $\hat{H}_2(t)$ in 3, acts during the T_2 -cycle (red dashed curve).

scribe the proposed spin model. In section II, we describe the emergence of DMBL. In section III, we numerically investigate the coexistence of time crystal and DMBL phases, and support our results analytically. In section IV, we look at long-time stability via regional magnetization and entanglement entropy for the system, and explore the robustness of this chimera against external static fields. Finally, we discuss our results and conclude.

I. THE MODEL AND SYSTEM DYNAMICS

We consider a one-dimensional spin-1/2 chain with N sites and transverse fields, with one field being static and the other harmonically driven in time. In the chain, all sites are connected via the Heisenberg interaction in the y spin axis. Now, we modulate the system in time by two repeating sequences of pulse waves, both with the same time periods T . The first sequence has a pulse width T_1 , and modulates the static transverse fields acting on the x spin axis. The second sequence has pulse width $T_2 = T - T_1$, and modulates both the interactions and time-periodic drive in the transverse field for the z spin axis. Thus, the full Hamiltonian is time-periodic with a period $T = T_1 + T_2$, and is given by,

$$\hat{H}(t) = \begin{cases} \hat{H}_1, & 0 \leq t < T_1, \\ \hat{H}_2, & T_1 \leq t < T, \end{cases} \quad (1)$$

where,

$$\hat{H}_1 = \hbar g(1 - \epsilon_A) \sum_{i \in A} \hat{\sigma}_i^x + \hbar g(1 - \epsilon_B) \sum_{i \in B} \hat{\sigma}_i^x + \hbar \hat{V}(\hat{\sigma}^\gamma), \quad (2)$$

$$\hat{H}_2(t) = \hbar \sum_{ij} J_{ij} \hat{\sigma}_i^y \hat{\sigma}_j^y + \hbar h_D \sum_i \hat{\sigma}_i^z + \hbar \hat{V}(\hat{\sigma}^\gamma), \quad (3)$$

and $\hat{\sigma}_i^{x,y,z}$ are the Pauli matrices at i -th site. Henceforth, we shall simplify our analysis by assuming that

the pulse waves modulating these Hamiltonians have a 50% duty-cycle, i.e. $T_1 = T_2 = T/2$. The Hamiltonian \hat{H}_1 in Eq 2 represents a transverse field that can perform spin-flips on spins polarized in the direction of the drive. To realize the DTC phase on the chain, we set an *ideal value* of this field to $g = \pi/T$. Now, we divide the chain into two physical regions denoted by A and B , based on two relative deviations $\epsilon_{A/B} \in [0, 1]$ of the field from this ideal value. Thus, these deviation parameters are *rotational errors* for the two regions, and play an essential role in differentiating between the two regions¹. The Hamiltonian \hat{H}_2 in Eq.(3) represents a standard long-range spin-chain in 1-dimension. The first term models the interaction between two sites ($i > j$) with a coupling strength J_{ij} , assumed to follow a power law decay $J_{ij} = J_0/|i - j|^\beta$. We have adapted Buyskikh's benchmarking [21] to classify the scaling of spin-spin interaction by varying β . According to this classification, when $\beta \in [0, 1]$, the interaction is classified as *long-range*, with $\beta = 0$ called the *all-to-all* interaction; the range $\beta \in (1, 2)$, as *intermediate-range* interaction; the range $\beta > 2$ as the *short range* interaction, with $\beta = \infty$ called the *nearest-neighbor* interaction. The second term in \hat{H}_2 is a continuous transverse time-periodic drive $\hat{H}_D = \hbar h_D \sum_i \hat{\sigma}_i^z$, where $h_D = -h \sin(\omega t)$, and

h, ω are the amplitude and frequency (respectively) of the drive. We have considered ω to be sufficiently high such that $\omega \gg J_0$. Experimentally, this can be accomplished using external high-frequency drives whose time-scales are significantly shorter than the relaxation rate due to the interactions in \hat{H}_2 . [8, 22–24]. At specific values of h and ω , our model shows a dynamical state that facilitates the manifestation of CDT/DL, which prevents the system from rapid thermalization. We will elaborate on this in section II. The final term in both $\hat{H}_{1,2}$, in Eqs. 2, and 3, is $\hat{V}(\hat{\sigma}^\gamma) \equiv \gamma \sum_{i=1}^N (\hat{\sigma}_i^x + \hat{\sigma}_i^y)$. It serves as a controlled additional static field that operates in the x and y spin axes. This term can also be interpreted as a static magnetic imperfection that is modulated by a parameter γ . We have chosen to ignore this by default, and re-introduce it in section IV in order to investigate the robustness of the chimera against such imperfections. We populate the spins in a fully polarized product state of up-spins, as depicted in the top panel of Fig. 2. During the T_1 -cycle of the pulses, the spins in region A *ideally* undergo a *spin-flip* resulting in a spin-down orientation, while the spins situated within region B, remain ideally unaltered. If the dynamics in the T_2 -cycle of the pulses remains localized by CDT/DL, this state of affairs is continued to the time $t = T$, as depicted in the next lower panel of Fig. 2. The localization ensures that each of the spins

¹ For instance, when $\epsilon_A \sim 0$ and $\epsilon_B \sim 1$, the field in region-A cause imperfect spin-flips, while that in region-B do not flip most spins.

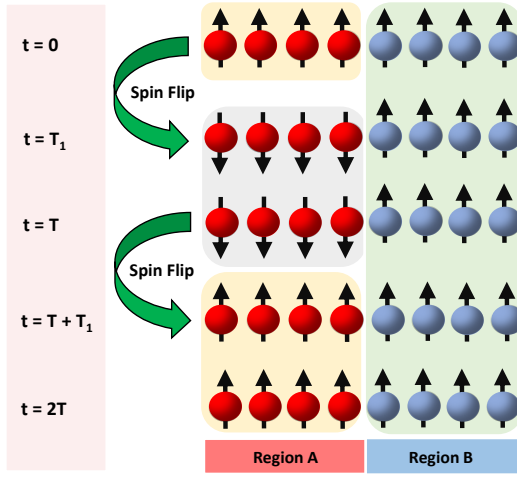


FIG. 2. Spin-flips that arise in the spin-1/2 chain due to the dynamics described in Eqs. 2 and 3, where the system is broken into two regions, A (left panels) and B (right panels). Snapshots at times $t = 0, T_1, T, T + T_1$ and $t = 2T$ are represented from the top to bottom panels respectively. The spins at region B remain unaltered for all time. In region A , spins are flipped at T_1 and preserved by CDT/DL during the T_2 -cycle until $t = T_1 + T_2 = T$. In the next T_1 -cycle, they are flipped back and preserved again by CDT/DL again until $t = 2T$. Thus, region A has a *period-doubling* response from $t = 0$ to $t = 2T$.

of the system are independent of each other, preventing any growth of correlations or entanglement between them during this cycle. Now, when the T_1 -cycle repeats, the spins are flipped back to their initial condition, while the dynamics remains localized during the next T_2 -cycle due to CDT/DL. Thus, when the system is driven up to the next time period $2T$, a spin magnetization *period doubling* [25, 26], or *half-frequency sub-harmonic* response is expected.

II. INTERACTING DYNAMICAL LOCALIZATION

Before investigating the chimera order in our model, we explain how the Hamiltonian \hat{H}_2 in Eq. (1) exhibits CDT/DL by analytically solving for the dynamics during all T_2 -cycles. During these times, the system is driven by a sinusoidal transverse periodic drive h_D as illustrated in Fig. 1.

Let us employ the *moving frame method* [14], where a unitary transformation is performed to the instantaneous rest frame of the rotation representing the drive. The transformation on the state yields $|\psi(t)\rangle_{\text{mov}} = \hat{U}^\dagger(t_0, t)|\psi(t)\rangle$, where

$$\hat{U}(t_0, t) \equiv \mathcal{T} e^{-\frac{i}{\hbar} \int_{t_0}^t dt' \hat{H}_D}. \quad (4)$$

During the first T_2 -cycle, $t \in \left[\frac{T}{2}, T\right]$. Thus,

$$\begin{aligned} \hat{U}(T/2, t) &= \exp \left[-\frac{i}{\hbar} \int_{T/2}^{t+T/2} (-h \sin(\omega t')) dt' \hbar \sum_i \hat{\sigma}_i^z \right] \\ &= \prod_i \exp \left[-i \hat{\sigma}_i^z \zeta(t) \right], \end{aligned} \quad (5)$$

$$\text{where, } \zeta(t) = h \int_{T/2}^{T/2+t} [-\sin(\omega t') dt'] = \frac{h}{\omega} [1 - \cos(\omega t)].$$

Now, in this ‘rotating frame’, the Hamiltonian transforms to [14],

$$\begin{aligned} \hat{H}^{\text{mov}}(t) &= \hat{U}^\dagger \hat{H}_2(t) \hat{U} - i \hat{U}^\dagger \partial_t \hat{U} \\ &= \hat{U}^\dagger [\hbar \sum_{ij} J_{ij} \hat{\sigma}_i^y \hat{\sigma}_j^y] \hat{U} \\ &= \hbar \sum_{ij} J_{ij} (\hat{\sigma}_i^y \hat{\sigma}_j^y) e^{i2\zeta(t) \hat{\sigma}_i^z} e^{i2\zeta(t) \hat{\sigma}_j^z} \end{aligned} \quad (6)$$

Next, we apply the *Jacobi Anger expansion*, $e^{iz \cos(\theta)} = \sum_{n=-\infty}^{\infty} \mathcal{J}_n(z) e^{in\theta}$, where \mathcal{J}_n 's denote the Bessel's function of first kind of n 'th order. This allows for a Fourier series expansion of $\hat{H}^{\text{mov}}(t)$. Now, we introduce Rotating Wave Approximation (RWA), which, in the high frequency limit, approximates the Fourier modes with their coarse-grained values over long times. This allows us to average out all but the zeroth Fourier mode (see Appendix A for details), resulting in the approximation,

$$\begin{aligned} \hat{H}^{\text{mov}}(t) &\approx \hat{H}^{\text{RWA}} = \hbar \sum_{ij} J_{ij} (\hat{\sigma}_i^y \hat{\sigma}_j^y) \mathcal{J}_0 \left(\frac{4h}{\omega} \right) \\ &\quad \left[1 \left\{ \mathcal{J}_0 \left(\frac{4h}{\omega} \right) + \cos \left(\frac{4h}{\omega} \right) \right\} - \hat{\sigma}_i^z \hat{\sigma}_j^z \left\{ \mathcal{J}_0 \left(\frac{4h}{\omega} \right) \right. \right. \\ &\quad \left. \left. - \cos \left(\frac{4h}{\omega} \right) \right\} + \frac{i}{2} (\hat{\sigma}_i^z + \hat{\sigma}_j^z) \sin \left(\frac{4h}{\omega} \right) \right]. \end{aligned} \quad (7)$$

Now, if the drive parameters h and ω are engineered in such a way that the ratio $4h/\omega$ lies at one of the roots of \mathcal{J}_0 ², it is possible to nullify the dynamics of \hat{H}_2 during all T_2 -cycles, hence inducing localization in the system. We have supported this result by numerical simulations, detailed in section IV A. There, $\hat{\sigma}^z$ is detected as an approximate integral invariant [12, 27].

III. COEXISTENCE OF DTC & DMBL

The occurrence of a chimera state in the model outlined in section I can be illustrated by employing *Floquet theory* to examine the dynamics at the stroboscopic

² This can be achieved when $\omega \gg J_0$ by ensuring that $h \gg J_0$.

times, namely, at integer multiples of the time period T .

The effective Floquet Hamiltonian for a system undergoing two periods can be written as follows:

$$H^{\text{eff}} \approx \frac{\hbar}{2} \sum_{l,m \in A} J_{lm} \hat{\sigma}_l^y \hat{\sigma}_m^y + \frac{\hbar \epsilon_A \pi}{4} \sum_{\substack{l,m \in A \\ l \neq m}} J_{lm} \hat{\sigma}_l^z \hat{\sigma}_m^y + \frac{\hbar}{2} \sum_{l,m \in B} J_{lm} \hat{\sigma}_l^y \hat{\sigma}_m^y + \frac{h\hbar}{\pi} \sum_{m \in B} \hat{\sigma}_m^z - \frac{\hbar \pi \epsilon_A}{4T} \sum_{l \in A} \left\{ \hat{\sigma}_l^x \left[\cos(\hat{\theta}_l) \cos\left(\frac{4h}{\omega}\right) + 1 \right] + \hat{\sigma}_l^y \cos(\hat{\theta}_l) \sin\left(\frac{4h}{\omega}\right) - \hat{\sigma}_l^z \sin(\hat{\theta}_l) \right\}. \quad (8)$$

Here, $\hat{\theta}_l \equiv 2 \left(\sum_{m \in B} J_{lm} \hat{\sigma}_m^y \frac{T}{2} \right)$ denotes a rotation acting on $\hat{\sigma}_l^y$, the local y -spin³. To examine the influence of rotational error on the chimera order, let us begin by considering the scenario when $\epsilon_A = 0$. In this situation, the effective Hamiltonian H^{eff} in Eq. (8) decouples into terms that live separately in regions A and B, *i.e.*,

$$H_{\epsilon_A=0}^{\text{eff}} = \frac{\hbar}{2} \left(\sum_{l,m \in A} J_{lm} \hat{\sigma}_l^y \hat{\sigma}_m^y + \sum_{l,m \in B} J_{lm} \hat{\sigma}_l^y \hat{\sigma}_m^y + \frac{2h}{\pi} \sum_{m \in B} \hat{\sigma}_m^z \right). \quad (9)$$

In such a case, the quantum dynamics of the two regions exhibit mutual independence when the system is first prepared in a state that can be factorized as a product of states in the invariant sub-spaces of regions A and B, respectively. It is crucial to note that no transfer or loss of quantum information occurs between these regions during the ensuing dynamics. Since we still have a significant degree of flexibility in selecting the driving parameters, it is possible to configure them in such a way as to induce DMBL in region B , while preserving a stable DTC in region A . Let us now increase the parameter ϵ_A while maintaining a sufficiently high frequency for the drive, so that it is possible to disregard the term $\hat{\theta}_l \approx 0$ due to the condition $T \ll \hbar/J_0$. Under these circumstances, the strength of the coupling between two regions is significantly influenced by the ratio χ , defined as $\chi \equiv 4h/\omega$. This dependence is characterized by the amplitudes $1 + \cos \chi$ and $\sin \chi$, which exhibit a non-monotonic behavior. Specifically, when χ takes the form of $(2n+1)\pi$, where n is a non-negative integer, the decoupling of regions A and B occurs again, regardless of the value of ϵ_A being non-zero. Therefore, it is anticipated that a DTC-DMBL chimera will exhibit a rather steady behavior when operating within proximity of this regime.

³ See Appendix B for details.

We now present visuals of the local magnetization, denoted as $\langle \hat{S}_i^z(t) \rangle$, which is equivalent to the expectation value of the operator $\hat{\sigma}_i^z$ with respect to the state $|\Psi(t)\rangle$, for all sites i in the spin-chain. The aforementioned data has been obtained using numerical simulations of the Schrödinger dynamics, represented by the equation $\dot{H}(t) |\Psi(t)\rangle = i\hbar \partial |\Psi(t)\rangle / \partial t$. This equation describes the behavior of the quantum many-body state $|\Psi(t)\rangle$. The simulations were conducted using QuTiP, a Python-based Quantum Toolbox [28]. The simulations were performed over extended duration (up to $t = 80T$, with \hbar normalized to unity) and across various ranges of power law interactions ($\beta = 0, 1.5, 2.5, \infty$). Additionally, simulations were conducted for both weak and strong interaction amplitudes ($J_0 = 0.072/T$ and $J_0 = 0.2/T$ respectively), which are similar to the parameters selected by Sakurai in a previous study [6]. To assess the durability of this chimera, we set the values of the rotational errors as $\epsilon_A = 0.03$ and $\epsilon_B = 0.9$. Furthermore, in order to observe the emergence of the chimera state in our model, we manipulate the periodic drive in $\hat{H}_2(t)$ by setting a high frequency $\omega = 20$ for two different scenarios: one where the parameter $\chi \equiv 4h/\omega$ is located at a root of the Bessel function $J_0(\chi)$, specifically at the CDT/DL point, and another where χ is at a distance from any roots.

As illustrated in Fig. 3, the local magnetization exhibits sub-harmonics with a frequency that is half of the driving frequency in region A at the CDT/DL point, under the condition of strong spin-spin coupling. Simultaneously, region B exhibits localized dynamics. As a result, the coexistence of the DTC and DMBL phases is observed in regions A and B, respectively, leading to the creation of a chimera state. Conversely, it is evident that the system dynamics demonstrate instability upon deviation from the CDT/DL point, irrespective of the particular values of J_0 that have been chosen. In a similar vein, it can be noted that the weak interactions demonstrate the presence of a stable chimera state when they possess a range that encompasses all spins ($\beta = 0$). However, when considering intermediate ($\beta = 1.5$), short ($\beta = 2.5$), and nearest-neighbor range interactions ($\beta = \infty$), the DTC melts rapidly inside region A, typically occurring

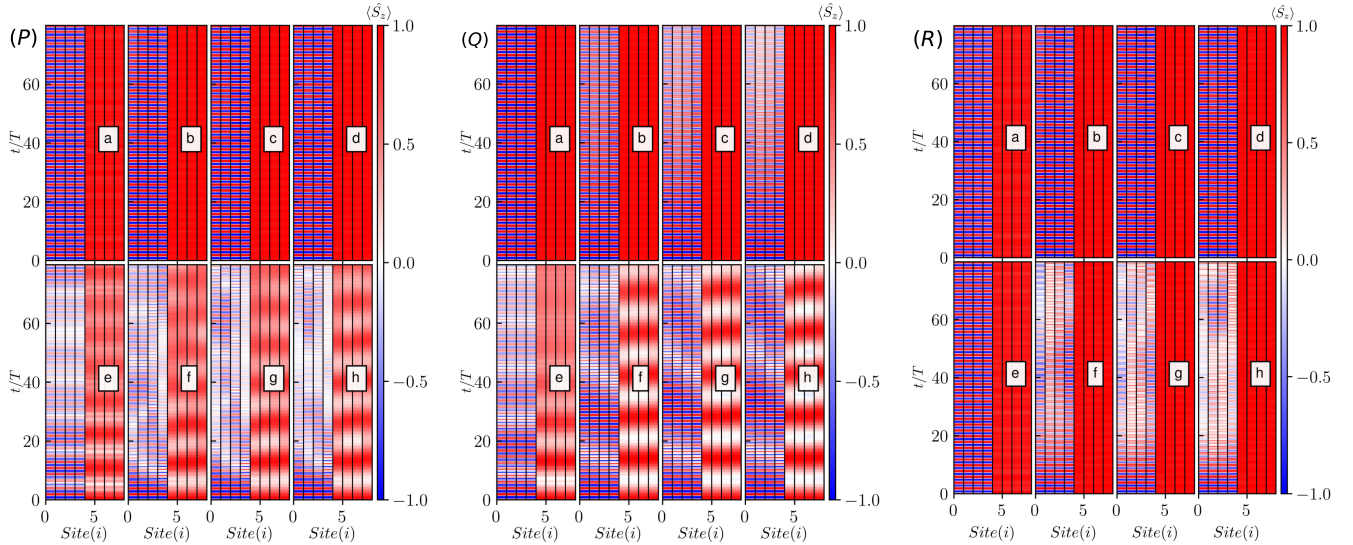


FIG. 3. The time evolution of local magnetization for each spin at region A ($\text{Site}(i)=0,1,2,3$) and region B ($\text{Site}(i)=4,5,6,7$) is plotted for $N = 8$ spins in a periodically driven one-dimensional spin chain, starting from a fully polarized spin state, with drive frequency $\omega = 20$. The spin rotation error $\epsilon_A = 0.03$ and $\epsilon_B = 0.9$, and $g = \pi/T$, where $T = 2\pi/\omega$ is the time period of the drive. In all three panels, different ranges of spin-interactions such as long-range($\beta = 0$), intermediate range($\beta = 1.5$), short range($\beta = 2.5$), and nearest neighbor range($\beta = \infty$), are chosen and plotted respectively from left to right, namely, (a, b,c,d) in the top row and (e,f,g,h) in the bottom row of each panel. The results from the time evolution for strong spin coupling ($J_0 = 0.2/T$) are shown in the left panel (P) and weak spin coupling ($J_0 = 0.027/T$) in the middle panel (Q). The top panels of P & Q show plots where the drive amplitude h is chosen such that the system lies at the lowest CDT/DL point and bottom panels show results away from that CDT/DL point. In the right panel (R), local magnetization for an effectively small spin rotational error $\epsilon_A = 0.05$ (top panel of R) and a larger $\epsilon_A = 0.1$ (bottom panel of R) are plotted at the same CDT/DL point. At small $\epsilon_A = 0.5$, the DTC-DMBL chimera is stable, while at $\epsilon_A = 0.1$, DTC is stable only for long-range interaction, but in other spin ranges, the DTC phase melts at larger times.

within 20 cycles of the drive. The results described in this study align with the conclusions published in previous research [6].

The stability of this DTC phase exhibits notable disparities between strong and weak coupling interactions. At the CDT/DL point, it is seen that the DTC phase exhibits enhanced stability in the presence of strong coupling compared to weak coupling, specifically for interactions that are not long-range in nature. The phenomenon of stable DTC is observed in long-range spin chains, regardless of the strength of spin interactions. Therefore, it is feasible to see the emergence of a chimera state consisting of two separate phases of matter, specifically a time crystal and a localized ferromagnet, simultaneously in a spin-chain system. This phenomenon can occur under typical experimental settings, with long-range interactions being the most suitable candidate. The suitability of long-range interactions was examined by analyzing the dynamics in frequency space (with the frequency variable denoted by Ω) by applying a Fast Fourier Transform (FFT) on the local magnetism at a specific spin site ($\text{site}(i) = 1$) in region A. The numerical FFT algorithms provided by the NumPy library were utilized to achieve this task [29]. The results are visually presented in Fig.4. The frequency Ω in the abscissas has been scaled relative to the driving frequency ω . The sub-harmonic response at $\Omega = \omega/2$ can be de-

tected by observing the peaks at half-integer multiples of ω . This observation serves as confirmation of the onset of discrete TTSB throughout all selected spin-interaction ranges. The stability of the resulting DTC will be influenced by the contributions originating from the underlying continuum of frequencies. When β approaches zero, the continuum exhibits a higher degree of submissiveness towards the sub-harmonic peaks compared to bigger values. This distinction is especially noticeable under conditions of weak coupling. Therefore, in the context of a DTC phase of matter, it is advantageous to consider long-range interactions rather than short-range interactions when selecting potential candidates. The present analysis is consistent with the numerical results shown in Fig.3, where each individual spin-interaction type provides evidence of a persistent and reliable DTC over an extended duration.

Additionally, we have conducted an analysis on the resilience of the DTC in the presence of larger rotational errors. The simulation results are presented in the panel situated on the rightmost side of Fig. 3. In the present simulations, we examine two distinct values for the parameter ϵ_A , namely $\epsilon_A = 0.05$ and $\epsilon_A = 0.1$, while maintaining a constant value of ϵ_B at 0.9. In this study, we investigate various ranges of interactions, denoted by the parameter β , which assumes the values of 0.0, 1.5, 2.5, and infinity. The aforementioned investiga-

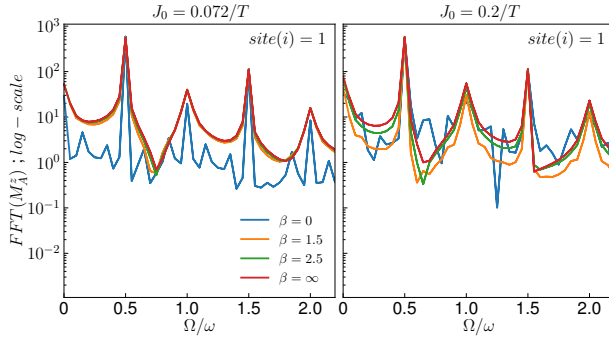


FIG. 4. Fast Fourier Transforms of the local magnetization at site $i = 1$ in region A of the spin-chain for weak coupling ($J_0 = 0.072/T$, left panel) and strong coupling ($J_0 = 0.2/T$, right panel) for different values of β as indicated in the legend. The amplitude h is adjusted so that the system is at the smallest CDT/DL point. All other parameters are the same as those in Fig 3. The peaks at half-integer multiples of ω denote sub-harmonic responses in region A resulting in stable DTC.

tions are carried out at a CDT/DL point under strong coupling, $J_0 = 0.2/T$. A steady DTC was observed for all interaction ranges when the value of ϵ_A was set to 0.05. The stability of the DTC is maintained for larger values of ϵ_A , namely when $\epsilon_A = 0.1$, when considering all-to-all interactions ($\beta = 0$). However, in the case of spin-spin interactions with other ranges, the DTC diminishes rapidly. This finding provides evidence in favor of the hypothesis that long-range interactions are the most advantageous for the development of a DTC-DMBL-chimera.

In order to examine dependencies on drive parameters, we have utilized numerical estimations of eigenvalues to represent the effective Hamiltonian H^{eff} . These are connected to the *Floquet quasi-energies* of the driven spin-chain, given by the eigenvalues of the time-dependent observable $\hat{H}(t) - i\hbar \partial/\partial t$ evaluated at $t = T$. The numerical diagonalization of the effective Hamiltonian H^{eff} has been performed for a system of $N = 8$ spins. The resulting quasi-energies have been displayed as a function of the parameter χ , defined as $\chi \equiv 4h/\omega$. The results are depicted in Fig. 5. The quasi-energy distribution displays a consistent pattern that is confined to the Floquet Brillouin Zone, namely the interval of $[-\frac{\pi}{2T}, \frac{\pi}{2T}]$, a consequence of Floquet's Theorem [17]. It is evident that the minimum repulsion between the quasienergies occurs when the parameter χ is an odd integer multiple of π . This finding provides empirical evidence that aligns with the theoretical arguments presented in the initial paragraph of this section. Consequently, it enables the separation of regions A and B, even in cases when $\epsilon_A \neq 0$. In contrast, in the scenario where $0 < \epsilon_A \ll 1$ and at the CDT/DL point where χ is situated on a root of $\mathcal{J}_0(\chi)$, it the coupling between regions A and B is fairly weak.

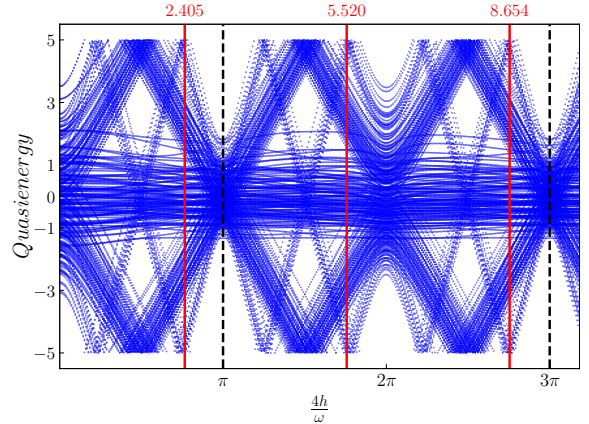


FIG. 5. Floquet quasi-energies of the driven spin-chain, estimated by numerically diagonalizing H^{eff} in Eq 8 for the one dimensional spin-1/2 chain. In these simulations, the number of spins $N = 8$. The system has open boundary conditions and strong coupling $J_0 = 0.2/T$. The quasi-energies are plotted for different values of h, ω , the amplitude and frequency of the periodic drive, respectively. The abscissa plots $4h/\omega$, where ω is kept constant and only h is changed, and the ordinate plots the corresponding quasi-energies. Level repulsion is minimum when $4h/\omega = (2n + 1)\pi$, $n \in \mathbb{N}_0$. The first such point is shown as a vertical black dashed line. The red solid lines indicate the roots of the zeroth order Bessel function $\mathcal{J}_0(\chi)$, i.e., CDT/DL points.

IV. STABILITY OF THE CHIMERA PHASE

In this section, we investigate the stability of the chimera phase in various regions of the complex parameter space. We observe simulations run for both strong and weak coupling with a wide variety of interaction ranges. The physical phenomena of interest involve the tunneling of any quantum information between the DTC and the DMBL regions that would serve to melt the DTC, and can be profiled by looking at the regional magnetization, as well as entanglement entropy between the regions, as functions of time. Finally, we investigate the robustness of the chimera against external static fields.

A. Regional Magnetization

We now examine the regional magnetization of the chimera state, which is given by the expectation value of the total z -spin in a specific region. This can enhance our understanding of the suitability of long-range interactions for the formation of stable time crystals. The expression for the magnetization of regions A and B is $M_{A/B}^z = \frac{2}{N} \sum_{i \in A/B} \langle \hat{\sigma}_i^z(t) \rangle$ [6].

We expanded the numerical simulations outlined in sec. III to encompass longer duration. Consequently, we acquired long-time estimates of the regional magnetization for regions A and B under varying conditions of spin

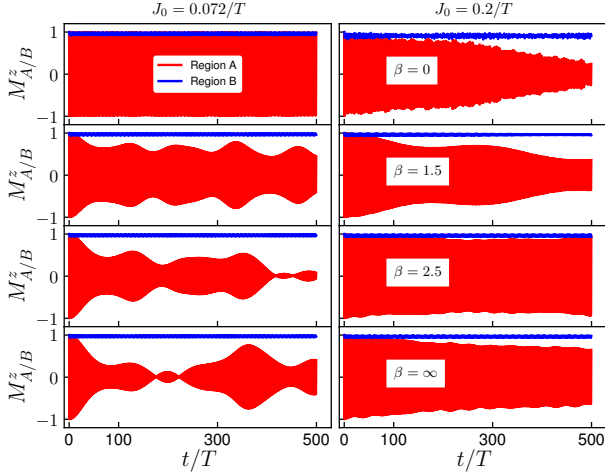


FIG. 6. Regional magnetization $M_{A/B}^z$ of the spin-chain. The magnetization of regions A (red) and B (blue) are plotted as functions of time t/T for both weak spin-coupling ($J_0 = 0.072/T$, left panels) and strong spin-coupling ($J_0 = 0.2/T$, right panels) and different ranges of spin interactions (characterized by β as specified in the legends). The time period is fixed by setting drive parameters h, ω to the first CDT/DL point, *i.e.* the first root of $\mathcal{J}_0(\chi)$. All other parameters are the same as the simulations visualized in Fig. 3.

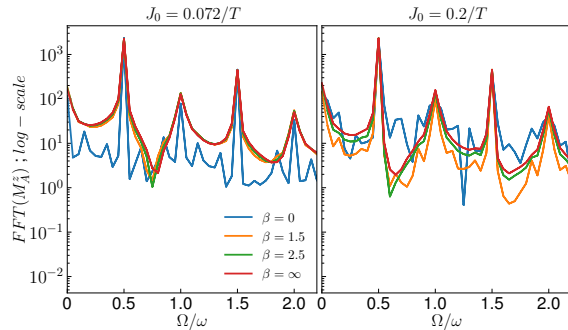


FIG. 7. FFT of regional magnetization M_A^z of the spin-chain. The magnetization of regions A are plotted as functions of time (ω/ω_D) for both weak spin-coupling ($J_0 = 0.072/T$, left panel) and strong spin-coupling ($J_0 = 0.2/T$, right panels) and different ranges of spin interactions (characterized by β as specified in the legends). The time period is fixed by setting drive parameters h, ω to the first CDT/DL point, *i.e.* the first root of $\mathcal{J}_0(\chi)$. All other parameters are the same as the simulations visualized in Fig. 3.

coupling strength and range. The results are plotted in Fig. 6. In both instances, the drive parameters were set to the CDT/DL point. In region B, the value of M_B^z remains constant at unity across all time for all ranges. In contrast, the behavior of M_A^z in region A is distinct. In the regime of weak coupling, the persistence of M_A^z is significant solely for all-to-all interactions, characterized by $\beta = 0$. However, for interactions at other ranges, M_A^z gradually dissipates with time. In the regime of high coupling, it can be observed that the DTC phase present

in region A undergoes a gradual dissolution over time, regardless of the range of spin interactions. The underlying mechanisms by which the DTC disintegrates can be investigated in frequency space via an FFT of the regional magnetization. The results, obtained in a manner similar to the FFTs of the site magnetization in sec III, are depicted in Fig. 7. In the regime of weak spin-coupling, the sub-harmonic peaks at $\Omega = \omega/2$ exhibit a dominant influence over the continuum of frequency responses in Ω . Consequently, this leads to a sustained regional magnetization over an extended period of time. As the parameter β is strengthened, the continuum of frequencies becomes more prominent, contributing to the faster disintegration of M_A^z . In the scenario of strong coupling, the continuum is more prominent across all ranges, leading to a more rapid disintegration of the regional magnetization compared to the weak spin-coupling.

B. Entanglement Entropy

In contrast to the preceding subsection, which focused on the examination of macroscopic observables, the current section delves into a more direct analysis of microscopic aspects through the consideration of entanglement entropy (EE). The EE is commonly employed as a measure to quantify the degree of entanglement exhibited by quantum states across invariant subspaces. It provides valuable insights pertaining to quantum correlations and the ability for information storage. The mathematical expression for the entanglement entropy, denoted as S_{AB} , between areas A and B, may be described using the von Neumann entropy [30, 31]. The density matrix of a pure state $|\psi\rangle$ is $\hat{\rho} = |\psi\rangle\langle\psi|$. The reduced density matrices (RDMs) for regions A and B, denoted as $\hat{\rho}_A$ and $\hat{\rho}_B$ respectively, are obtained by taking the partial traces of $\hat{\rho}$ with respect to the complementary regions. Specifically, $\hat{\rho}_A$ is obtained by tracing out region B, *i.e.*, $\hat{\rho}_A \equiv \text{Tr}_B(\hat{\rho})$, while $\hat{\rho}_B \equiv \text{Tr}_A(\hat{\rho})$. The entanglement entropy (EE) is determined by

$$S_{AB} = -\text{Tr} [\hat{\rho}_A \ln (\hat{\rho}_A)] = -\text{Tr} [\hat{\rho}_B \ln (\hat{\rho}_B)]. \quad (10)$$

We have extended previous simulations to a later time point of $t = 2000 T$, and then calculated the EE for each time point. The results are plotted in Fig. 8 for both weak and strong spin coupling, while maintaining the driving parameters consistently at a CDT/DL point. The EE is found to start rising from the onset of the first T_2 -cycle, when the spin-interactions begin to impact the behavior of the spin-chain. The increase in EE is observed to be gradual even after prolonged interactions. The EE exhibits a more rapid increase in the case of strong spin coupling compared to weak spin coupling. As evidenced by Eq.(8), the coupling present in the effective Hamiltonian is directly proportional to the rotational error ϵ_A . When the value of ϵ_A is modest, it effectively hinders the interaction between regions A and B, hence inhibiting the increase of EE. This corroborates the results depicted in

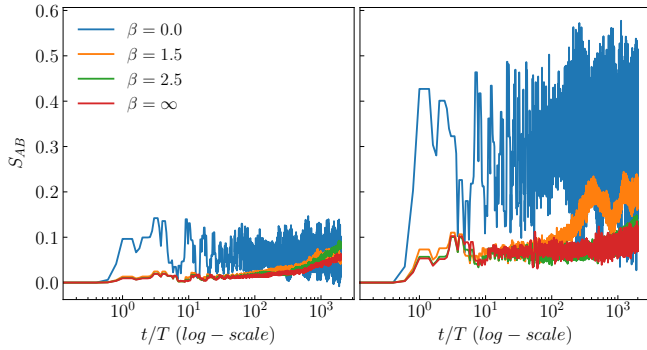


FIG. 8. Time evolution of Entanglement Entropy S_{AB} between regions A and B as a function of time at the CDT/DL point. The left panels plot results for weak spin coupling, and the right panels for stronger spin couplings. The corresponding values of J_0 are the same as those in Fig. 6, and all other parameters are identical to previous simulations. The spin-spin coupling interaction in \hat{H}_2 during T_2 leads to the onset of a rise in EE. The growth rate of the subject in question remains notably slow, persisting even up to $t = 2000 T$.

Fig.7, where the DTC appears to be more stable at weak coupling than strong coupling.

When thermalized at infinite temperature, the EE is extensive, and averages to $\langle \overline{S_{AB}} \rangle_T \rightarrow [N \ln 2 - 1] / 2$ [32]. When localized, the EE per particle vanishes in the thermodynamic limit. For finite sizes, it can be approximated as $\langle \overline{S_{AB}} \rangle_L \approx \ln 2$ [6]. In our spin chain, $N = 8$, yielding theoretical expressions, $\langle \overline{S_{AB}} \rangle_T \approx 2.27$, and $\langle \overline{S_{AB}} \rangle_L \approx 0.69$. The numerical values of the entanglement entropy (EE) are found to remain approximately in the range of $\in [0, 0.6]$, as can be seen in Fig.8. This observation indicates that the entire system remains athermal and localized, even when a significant amount of time has elapsed.

C. Robustness against Static Fields

The influence of the driving parameters h, ω significantly affects the long-lasting stability of the DTC-DMBL chimera. The strength of the chimera order diminishes even if there is a minor deviation from the CDT/DL point. This raises questions about the mechanisms by which the chimera resists external fields, even while functioning precisely at the CDT/DL point. In order to conduct an investigation, we will now incorporate the static field $\hbar \hat{V}(\hat{\sigma}^\gamma)$ discussed in section I into the Hamiltonian $\hat{H}(t)$. The aforementioned field remains un-modulated by the pulses and acts on the system identically at all times. Simulations were conducted using this field at a CDT/DL point, while maintaining all other parameters at the same values as in earlier simulations. These simulations were conducted for both strong ($\gamma = J_0 = 0.2/T$) and weak ($\gamma = J_0/5 = 0.2/5T$) field

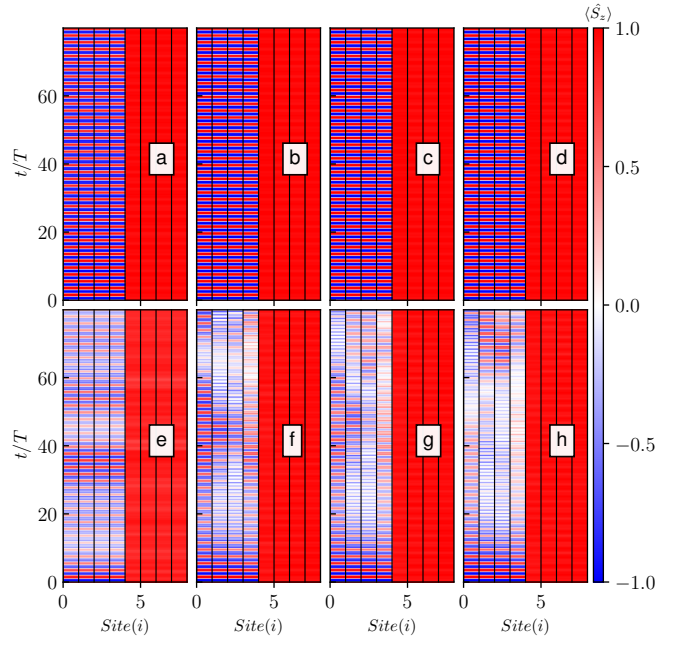


FIG. 9. Weak (top panels) and strong (bottom panels) additional static fields defined by $\gamma = J_0/5, J_0$ respectively ($J_0 = 0.2/T$), are applied in addition to the strong spin coupling and transverse field at different interaction ranges set by $\beta = 0.0$ (panels a,e), $\beta = 1.5$ (panels b,f), $\beta = 2.5$ (panels c,g), and $\beta = \infty$ (panels d,h). The local magnetization for each site (i) is plotted from $t = 0$ to $t = 80T$.

amplitudes. The findings are displayed in Fig. 9. At low values of γ , the influence of spin-interactions is more significant compared to the static field, leading to the continued existence of dynamical localization. Consequently, a stable chimera state of the DTC is observed. Nevertheless, when the value of γ increases, the static field becomes dominant over the interactions, resulting in the melting of the DTC after a few cycles. However, it is worth noting that the DMBL phase continues to exist even in the presence of the static field. Therefore, a chimera phase known as *Thermal-DMBL* becomes apparent at longer time scales. Therefore, it is possible to achieve a strong DTC-DMBL hybrid even when external fields are present.

V. DISCUSSION AND CONCLUSION

A quantum chimera state has been discovered, wherein a Discrete Time Crystal (DTC) and a Dynamically Many-Body Localized (DMBL) phase coexist on a one-dimensional spin-1/2 chain. This was accomplished by applying dynamical spin-flips regionally (with two regions labeled ‘A’ and ‘B’), followed by dynamical localization with a high-frequency periodic drive tuned to CDT/DL points determined by particular values of the drive parameters. The findings from numerical simula-

tions suggest that the DTC does not exhibit long-term persistence when weak spin coupling is present, especially in the case of all-to-all interaction ranges. The presence of a robust spin coupling hinders the relaxation of spins away from the desired DTC, stabilizing the phase regionally for long times throughout all interaction ranges. The stability of the DTC in region A is contingent upon the stability of the DMBL phase in region B. The long-range spin interaction is very robust against the exchange energy per spin, and enable the chimera to persist for both weak and strong coupling. We tuned the spin rotational error at region A and found that the chimera can persist only at small rotational error ϵ_A . The inter-region interaction term in the effective Floquet Hamiltonian in Eq. 8 is directly proportional to the spin rotation error denoted as ϵ_A . In the case of a significant value of ϵ_A , there is an increased level of coupling between the two regions. This heightened coupling results in the immediate melting of the DTC for all interactions, except for those that are long-range in nature.

To further study the resilience of this chimera against static perturbations, an additional external static field was included. Numerical simulations have demonstrated that the system is robust in the face of minor perturbations, as evidenced by the sustained presence of the DTC phase inside region A over an extended duration. However, when subjected to more significant perturbations, the system's robustness diminishes, leading to rapid dissolution of the DTC phase across all spin-interaction types. The Floquet Hamiltonian, obtained analytically, illustrates the occurrence of period-doubling sub-harmonic solutions to the Schrödinger dynamics. These solutions arise specifically at the reversal of global ferromagnetic order in the spin chain. This

conclusion is substantiated by exact simulations. The entanglement entropy rises at a very slow rate for both weak and strong regional spin interactions. Hence, the entire system is effectively prevented from undergoing thermalization, even in cases where the DTC phase disintegrates inside region A. The aforementioned property can be employed as quantum memory in various applications, as well as in the development of exceptionally accurate quantum clocks. The experimental realization of the suggested model and dynamics can be achieved using trapped ions, as demonstrated in previous studies [6, 33].

To summarize, we examined the various components that contribute to the stability of the DTC-DMBL-chimera order. Long-range spin interactions have been identified as the optimal choice for constructing the chimera. The scope of our analysis encompasses various magnitudes of power-law decay in spin-spin contacts, the magnitude of regional spin rotational error, the intensity of spin-coupling interactions, the presence of an extra external static field, and the parameters associated with the periodic drive. The aforementioned contributions play a key role in ensuring the stability of the chimera order.

ACKNOWLEDGMENTS

MR acknowledges The University of Burdwan for support via state-funded fellowship. AR acknowledges support from the University Grants Commission (UGC) of India, via BSR Startup Grant No. F.30-425/2018(BSR), also from the Science and Engineering Research Board (SERB, Govt. of India) Core Research Grant No. CRG/2018/004002.

-
- [1] Y. Kuramoto and D. Battogtokh, Nonlinear Phenomena in Complex Systems **5**, 380 (2002).
 - [2] M. J Panaggio and D. M Abrams, Nonlinearity **28**, R67 (2015).
 - [3] F. Parastesh, S. Jafari, H. Azarnoush, Z. Shahriari, Z. Wang, S. Boccaletti, and M. Perc, Physics Reports **898**, 1 (2021).
 - [4] V. M. Bastidas, I. Omelchenko, A. Zakharova, E. Schöll, and T. Brandes, Phys. Rev. E **92**, 062924 (2015).
 - [5] R. Singh, S. Dasgupta, and S. Sinha, Europhysics Letters **95**, 10004 (2011).
 - [6] A. Sakurai, V. M. Bastidas, W. J. Munro, and K. Nemoto, Phys. Rev. Lett. **126**, 120606 (2021).
 - [7] D. V. Else, B. Bauer, and C. Nayak, Phys. Rev. Lett. **117**, 090402 (2016).
 - [8] J. Zhang, P. W. Hess, A. Kyprianidis, P. Becker, A. Lee, J. Smith, G. Pagano, I.-D. Potirniche, A. C. Potter, A. Vishwanath, N. Y. Yao, and C. Monroe, Nature **543**, 217 (2017).
 - [9] F. Alet and N. Laflorencie, Comptes Rendus Physique **19**, 498 (2018).
 - [10] J. Smith, A. Lee, P. Richerme, B. Neyenhuis, P. W. Hess, P. Hauke, M. Heyl, D. A. Huse, and C. Monroe, Nature Physics **12**, 907 (2016).
 - [11] T. Nguyen, N. Andrejevic, H. C. Po, Q. Song, Y. Tsurimaki, N. C. Drucker, A. Alatas, E. E. Alp, B. M. Leu, A. Cunsolo, Y. Q. Cai, L. Wu, J. A. Garlow, Y. Zhu, H. Lu, A. C. Gossard, A. A. Puretzky, D. B. Geohegan, S. Huang, and M. Li, Nano Letters **21**, 7419 (2021).
 - [12] A. C. Keser, S. Ganeshan, G. Refael, and V. Galitski, Phys. Rev. B **94**, 085120 (2016).
 - [13] A. Haldar and A. Das, Annalen der Physik **529**, 1600333 (2017).
 - [14] A. Haldar, D. Sen, R. Moessner, and A. Das, Phys. Rev. X **11**, 021008 (2021).
 - [15] S. Bhattacharyya, A. Das, and S. Dasgupta, Phys. Rev. B **86**, 054410 (2012).
 - [16] S. Aditya and D. Sen, (2023), arXiv:2305.06056 [cond-mat.stat-mech].
 - [17] T. Nag, S. Roy, A. Dutta, and D. Sen, Phys. Rev. B **89**, 165425 (2014).
 - [18] A. Das, Phys. Rev. B **82**, 172402 (2010).
 - [19] F. Grossmann, T. Dittrich, P. Jung, and P. Hänggi, Phys. Rev. Lett. **67**, 516 (1991).

- [20] Y. Kayanuma and K. Saito, Phys. Rev. A **77**, 010101 (2008).
- [21] A. S. Buyskikh, M. Fagotti, J. Schachenmayer, F. Essler, and A. J. Daley, Phys. Rev. A **93**, 053620 (2016).
- [22] S. Choi, J. Choi, R. Landig, G. Kucsko, H. Zhou, J. Isoya, F. Jelezko, S. Onoda, H. Sumiya, V. Khemani, C. von Keyserlingk, N. Y. Yao, E. Demler, and M. D. Lukin, Nature **543**, 221 (2017).
- [23] J. I. Cirac and P. Zoller, Phys. Rev. Lett. **74**, 4091 (1995).
- [24] R. Blatt and C. F. Roos, Nature Physics **8**, 277 (2012).
- [25] J. Rovny, R. L. Blum, and S. E. Barrett, Phys. Rev. B **97**, 184301 (2018).
- [26] Y. Pan and B. Wang, Phys. Rev. Res. **2**, 043239 (2020).
- [27] V. V. Dodonov and V. I. Man'ko, Physica A: Statistical Mechanics and its Applications **94**, 403 (1978).
- [28] J. R. Johansson, P. D. Nation, and F. Nori, Computer Physics Communications **184**, 1234 (2013).
- [29] C. R. Harris, K. J. Millman, S. J. van der Walt, R. Gommers, P. Virtanen, D. Cournapeau, E. Wieser, J. Taylor, S. Berg, N. J. Smith, R. Kern, M. Picus, S. Hoyer, M. H. van Kerkwijk, M. Brett, A. Haldane, J. F. del Río, M. Wiebe, P. Peterson, P. Gérard-Marchant, K. Sheppard, T. Reddy, W. Weckesser, H. Abbasi, C. Gohlke, and T. E. Oliphant, Nature **585**, 357 (2020).
- [30] A. Bayat, S. Bose, and H. Johannesson, eds., Entanglement in Spin Chains, Quantum Science and Technology (Springer Cham, 2022).
- [31] T. Mendes-Santos, G. Giudici, R. Fazio, and M. Dalmonte, New Journal of Physics **22**, 013044 (2020).
- [32] T.-C. Lu and T. Grover, PRX Quantum **2**, 040319 (2021).
- [33] A. Friedenauer, H. Schmitz, J. T. Glueckert, D. Porras, and T. Schaetz, Nature Physics **4**, 757 (2008).
- [34] A. Haldar and A. Das, Journal of Physics: Condensed Matter **34**, 234001 (2022).
- [35] G. Arfken, H. Weber, and F. E. Harris, Mathematical Methods for Physicists, 7th ed. (Academic Press, 2011).
- [36] A. Eckardt and E. Anisimovas, New Journal of Physics **17**, 093039 (2015).
- [37] W. Magnus, Communications on Pure and Applied Mathematics **7**, 649 (1954).

Appendix A: DMBL in T_2 time interval

Let us consider a one-dimensional spin-1/2 chain consisting of N spins, with Heisenberg exchange interaction between them. The interaction follows a power law decay rule, where the exchange energy between the i^{th} and j^{th} spins is presumed to be $J_{ij} = J_0|i - j|^{-\beta}$. Let us now divide the chain into two regions, A and B, and introduce time dependencies via two pulse wave sequences in the manner described in sec. I and Fig 1. The first sequence induces spin-flips in region A within time T_1 , and the second modulates a global sinusoidal periodic drive in the field $s.t.$ $h_D = -h \sin(\omega t)$ within time T_2 , chosen to be such that the time period $T \equiv 2\pi/\omega = T_1 + T_2$. This drive parameters are controlled in such a way that the system is dynamically localized during the T_2 -cycles.

The Hamiltonian during the T_2 -cycle is $\hat{H}_2(t) = \hbar \sum_{i>j} J_{ij} \hat{\sigma}_i^y \hat{\sigma}_j^y - \hbar h \sin(\omega t) \sum_i \hat{\sigma}_i^z$. Let us define the free propagator

$$\hat{U}(t) \equiv \exp \left[-\frac{i}{\hbar} \int_{\frac{T}{2}}^{\frac{T}{2}+t} (-h \sin(\omega t')) dt' \hbar \sum_i \hat{\sigma}_i^z \right] = \prod_i \exp [-i \hat{\sigma}_i^z \zeta(t)], \quad (\text{A1})$$

where, $\zeta(t) = h \int_{\frac{T}{2}}^{\frac{T}{2}+t} (-\sin(\omega t') dt') = \frac{h}{\omega} (1 - \cos(\omega t))$. Now, the Hamiltonian can be transformed to the moving frame as follows [34].

$$\begin{aligned} \hat{H}^{mov}(t) &= \hat{U}^\dagger(t) \hat{H}_2(t) \hat{U}(t) - i \hat{U}^\dagger(t) \partial_t \hat{U}(t) \\ &= \prod_i \exp [-i \hat{\sigma}_i^z \zeta(t)] [\hbar \sum_{ij} J_{ij} \hat{\sigma}_i^y \hat{\sigma}_j^y] \exp [i \hat{\sigma}_i^z \zeta(t)] \\ &= \hbar \sum_{ij} J_{ij} e^{-i \hat{\sigma}_i^z \zeta(t)} e^{-i \hat{\sigma}_j^z \zeta(t)} (\hat{\sigma}_i^y \hat{\sigma}_j^y) e^{i \hat{\sigma}_i^z \zeta(t)} e^{i \hat{\sigma}_j^z \zeta(t)} \\ &= \hbar \sum_{ij} J_{ij} (\hat{\sigma}_i^y \hat{\sigma}_j^y) e^{i 2 \hat{\sigma}_i^z \zeta(t)} e^{i 2 \hat{\sigma}_j^z \zeta(t)} \\ &= \hbar \sum_{ij} J_{ij} (\hat{\sigma}_i^y \hat{\sigma}_j^y) [\mathbb{1} \cos^2(2\zeta) - \hat{\sigma}_i^z \hat{\sigma}_j^z \sin^2(2\zeta) + i(\hat{\sigma}_i^z + \hat{\sigma}_j^z) \cos(2\zeta) \sin(2\zeta)]. \end{aligned} \quad (\text{A2})$$

Here, we have utilized the expression, $\exp[i\hat{a}(\hat{n} \cdot \vec{\sigma})] = \mathbb{1} \cos(a) + i(\hat{n} \cdot \vec{\sigma}) \sin(a)$. Now, we invoke the Jacobi-Anger formula $e^{iz \cos(\omega t)} = \sum_{n=-\infty}^{\infty} \mathcal{J}_n(z) e^{in\omega t}$ [35], where $\mathcal{J}_n(z)$ is the Bessel function of the first kind of n^{th} order, and apply to the RHS of Eq. A2. This produces a Fourier series expansion for $\hat{H}^{mov}(t)$ with period ω . Note however, that the drive parameters h and ω are independent of each other. In high frequency limit, where $\omega \gg J_0$, the Rotating Wave Approximation (RWA) allows for approximating the Fourier modes with their long time coarse-grain averages. This provides us with the option to average all the Fourier modes to zero, except for the zeroth order mode. Thus, the \hat{H}^{mov} reduces to the RWA-Hamiltonian (\hat{H}^{RWA}),

$$\hat{H}^{mov} \approx \hat{H}^{RWA} = \hbar \sum_{ij} J_{ij} (\hat{\sigma}_i^y \hat{\sigma}_j^y) \mathcal{J}_0(\chi) \left\{ \mathbb{1} [\mathcal{J}_0(\chi) + \cos(\chi)] - \hat{\sigma}_i^z \hat{\sigma}_j^z [\mathcal{J}_0(\chi) - \cos(\chi)] + \frac{i}{2} (\hat{\sigma}_i^z + \hat{\sigma}_j^z) \sin(\chi) \right\}. \quad (\text{A3})$$

Now, for a particular ω , if h is controlled in such fashion that $\chi \equiv \frac{4h}{\omega}$ lies on one of the roots of $\mathcal{J}_0(\chi)$, then \hat{H}^{RWA} vanishes, resulting in localization of any initial state during the T_2 -cycles. This can be accomplished in various ways, for instance, if $\omega \gg J_0$, ensuring that $h \gg J_0$ such that $4h/\omega$ is of $\mathcal{O}(1)$ allows for the possibility of χ falling on the first root of $\mathcal{J}_0(\chi)$ even for large ω .

Appendix B: Effective Floquet Hamiltonian

Floquet theory is a widely used methodology for evaluating the behavior of time-periodic systems. In a quantum system that is time periodic with period T , the Hamiltonian obeys $\hat{H}(t+T) = \hat{H}(t) \forall t$. If we split the time-dependent part from the time-independent, or *d.c.* part, we can write

$$\hat{H}(t) = \hat{H}_0 + \varepsilon \hat{H}_1(t)$$

The corresponding propagator can be obtained by solving the Schrödinger equation $i\hbar\partial_t\hat{U}(t) = \hat{H}(t)\hat{U}(t)$. The propagator at $t = T$, given by $\hat{\mathcal{F}} \equiv \hat{U}(T)$ is called the *Floquet operator*. Now, it follows from Floquet's Theorem that, if the system is strobed at integer multiples of T , the dynamics can be mapped to that of a time-independent effective Hamiltonian \hat{H}_F , such that $\hat{U}(nT) = \exp\left[-\frac{i}{\hbar}\hat{H}_F nT\right]$ [36]. The operator \hat{H}_F (also denoted by H^{eff}) is obtained from

the original time-dependent Hamiltonian, and is given by, $\hat{H}_F = \left(\hat{H}(t) - i\hbar\frac{\partial}{\partial t}\right)$ evaluated at $t = T$.

Now, the proposed spin chain in Eq.(1) needs to evolve for at least two time periods to manifest a DTC. If the effective time-independent Hamiltonian at that time is denoted by $\hat{H}_{\epsilon_A,2T}^{\text{eff}}$, then, the propagator

$$\hat{\mathcal{F}}^2 \equiv \exp\left(-\frac{i}{\hbar}\hat{H}_{\epsilon_A,2T}^{\text{eff}} 2T\right) \quad (\text{B1})$$

$$= \mathcal{T} \exp\left(-\frac{i}{\hbar} \int_{\frac{3T}{2}}^{2T} \hat{H}_2(t) dt\right) \exp\left(-\frac{i}{\hbar} \hat{H}_1 T_1\right) \mathcal{T} \exp\left(-\frac{i}{\hbar} \int_{\frac{T}{2}}^T \hat{H}_2(t) dt\right) \exp\left(-\frac{i}{\hbar} \hat{H}_1 T_1\right). \quad (\text{B2})$$

Here \mathcal{T} denotes the time-ordering operation. To evaluate $\hat{\mathcal{F}}^2$, we start by calculating each of the four terms in RHS of Eq.B2. During the T_1 -cycle, $t \in [0, T/2]$, and the time-independent Hamiltonian \hat{H}_1 is applied on spin chain. Thus,

$$\exp\left(-\frac{i}{\hbar} \hat{H}_1 T_1\right) = \exp\left[\frac{-i(1-\epsilon_A)\pi}{2} \sum_{l \in A} \hat{\sigma}_l^x\right]. \quad (\text{B3})$$

It is evident that the effective Hamiltonian for $t \in [T, 3T/2]$ will be same as that obtained from Eq.(B3). Next, during the T_2 -cycle, $t \in [T/2, T]$, and the time-dependent Hamiltonian, $\hat{H}_2(t)$ is applied. Therefore,

$$\begin{aligned} \mathcal{T} \exp\left(-\frac{i}{\hbar} \int_{\frac{T}{2}}^T \hat{H}_2(t) dt\right) &= \exp\left(-\frac{i}{\hbar} \int_{\frac{T}{2}}^T \left[\hbar \sum_{i \neq j} J_{ij} \hat{\sigma}_i^y \hat{\sigma}_j^y - \hbar h \sin(\omega t) \sum_i \hat{\sigma}_i^z\right] dt\right) \\ &= \exp\left(-i \left[\sum_{i \neq j} J_{ij} \hat{\sigma}_i^y \hat{\sigma}_j^y \frac{T}{2} + \frac{2h}{\omega} \sum_i \hat{\sigma}_i^z \right]\right) \end{aligned} \quad (\text{B4})$$

Clearly, the effective Hamiltonian for the times $t \in [3T/2, 2T]$ will also be the same. Now, let us consider the case where $\epsilon_A \neq 0$ and $\epsilon_B = 1$. Furthermore, let us define the operators $\hat{V}_{\epsilon_A} \equiv \exp\left(\frac{i\epsilon_A\pi}{2} \sum_{l \in A} \hat{\sigma}_l^x\right)$, $\hat{\theta}_l \equiv 2 \left(\sum_{m \in B} J_{lm} \hat{\sigma}_m^y \frac{T}{2} \right)$; the latter describes a rotation acting on operator $\hat{\sigma}_l^y$ in only region B. Now, we can expand expression for the T_2 -cycle propagator in Eq. B4 by splitting the contributions from regions A and B. This yields

$$\begin{aligned} \mathcal{T} \exp\left\{-\frac{i}{\hbar} \int_{\frac{T}{2}}^T \hat{H}_2(t) dt\right\} &= \exp\left\{-i \left[\sum_{l,m \in A} J_{lm} \hat{\sigma}_l^y \hat{\sigma}_m^y + \sum_{l,m \in B} J_{lm} \hat{\sigma}_l^y \hat{\sigma}_m^y + \sum_{\substack{l \in A, \\ m \in B}} J_{lm} \hat{\sigma}_l^y \hat{\sigma}_m^y \right.\right. \\ &\quad \left.\left. + \frac{4h}{\omega T} \left(\sum_{l \in A} \hat{\sigma}_l^z + \sum_{m \in B} \hat{\sigma}_m^z \right) \right] \frac{T}{2} \right\}. \quad (\text{B5}) \end{aligned}$$

Substituting the RHS of Eqs.(B3) & (B5) into the RHS of Eq. (B2) yields

$$\begin{aligned} \hat{\mathcal{F}}^2 &= \exp\left\{-i \left[\sum_{l,m \in A} J_{lm} \hat{\sigma}_l^y \hat{\sigma}_m^y \frac{T}{2} + \sum_{l,m \in B} J_{lm} \hat{\sigma}_l^y \hat{\sigma}_m^y \frac{T}{2} + \sum_{\substack{l \in A, \\ m \in B}} J_{lm} \hat{\sigma}_l^y \hat{\sigma}_m^y \frac{T}{2} + \frac{2h}{\omega} \left(\sum_{l \in A} \hat{\sigma}_l^z + \sum_{m \in B} \hat{\sigma}_m^z \right) \right] \right\} \hat{V}_{\epsilon_A} \\ &\quad \exp\left\{-i \left[\sum_{l,m \in A} J_{lm} \hat{\sigma}_l^y \hat{\sigma}_m^y \frac{T}{2} + \sum_{l,m \in B} J_{lm} \hat{\sigma}_l^y \hat{\sigma}_m^y \frac{T}{2} - \sum_{\substack{l \in A, \\ m \in B}} J_{lm} \hat{\sigma}_l^y \hat{\sigma}_m^y \frac{T}{2} + \frac{2h}{\omega} \left(- \sum_{l \in A} \hat{\sigma}_l^z + \sum_{m \in B} \hat{\sigma}_m^z \right) \right] \right\} \hat{V}_{\epsilon_A}. \end{aligned}$$

We can simplify this expression further with the approximation that all operators with norms $\mathcal{O}(T^2)$ can be neglected in comparison to those with norm $\sim T$ for sufficiently large $\omega \equiv 2\pi/T$. Thus, for instance, $e^{T\hat{A}+T\hat{B}} =$

$e^{T\hat{A}} e^{T\hat{B}} e^{C_2 T^2 [\hat{A}, \hat{B}]} e^{C_3 T^3 [\hat{A}, [\hat{A}, \hat{B}]]} \dots \approx e^{T\hat{A}} e^{T\hat{B}}$, once all higher order operators are neglected after applying the Zassenhaus' formula [37]. This yields

$$\begin{aligned} \hat{\mathcal{F}}^2 &\approx \exp \left[-i \sum_{l,m \in A} J_{lm} \hat{\sigma}_l^y \hat{\sigma}_m^y \frac{T}{2} \right] \exp \left[-i \left(\frac{2h}{\omega} \sum_{l \in A} \hat{\sigma}_l^z + \sum_{l \in A} \frac{\hat{\theta}_l}{2} \hat{\sigma}_l^y \right) \right] \\ &\quad \hat{V}_{\epsilon_A} \exp \left[i \left(\sum_{l \in A} \frac{\hat{\theta}_l}{2} \hat{\sigma}_l^y + \frac{2h}{\omega} \sum_{l \in A} \hat{\sigma}_l^z \right) \right] \exp \left[-i \sum_{l,m \in A} J_{lm} \hat{\sigma}_l^y \hat{\sigma}_m^y \frac{T}{2} \right] \exp [-iH_B T] \hat{V}_{\epsilon_A}, \end{aligned}$$

where, for the sake of brevity, we have defined the T_2 -cycle Hamiltonian in region-B, $H_B \equiv \sum_{l,m \in B} J_{lm} \hat{\sigma}_l^y \hat{\sigma}_m^y + \frac{4h}{\omega T} \sum_{m \in B} \hat{\sigma}_m^z$. We now observe that $\hat{\theta}_l$ commutes with all operators that live in region-A, thus allowing us to temporarily treat it as a c -number in algebraic manipulations, allowing for the simplification

$$\begin{aligned} \hat{\mathcal{F}}^2 &\approx \exp \left[-2i \sum_{l,m \in A} J_{lm} \hat{\sigma}_l^y \hat{\sigma}_m^y \frac{T}{2} \right] \exp \left[\frac{i\epsilon_A \pi}{2} \sum_{l \in A} \left\{ \hat{\sigma}_l^x \cos(\hat{\theta}_l) \cos\left(\frac{4h}{\omega}\right) \right. \right. \\ &\quad \left. \left. + \hat{\sigma}_l^y \cos(\hat{\theta}_l) \sin\left(\frac{4h}{\omega}\right) - \hat{\sigma}_l^z \sin(\hat{\theta}_l) \right\} \right] \exp [-iH_B T] \hat{V}_{\epsilon_A} \\ &= \exp \left[-2i \sum_{l,m \in A} J_{lm} \hat{\sigma}_l^y \hat{\sigma}_m^y \frac{T}{2} \right] \exp \left(\frac{i\epsilon_A \pi}{2} \sum_{l \in A} \hat{\sigma}_l^x \right) \exp \left[\frac{i\epsilon_A \pi}{2} \sum_{l \in A} \left\{ \hat{\sigma}_l^x \cos(\hat{\theta}_l) \cos\left(\frac{4h}{\omega}\right) \right. \right. \\ &\quad \left. \left. + \hat{\sigma}_l^y \cos(\hat{\theta}_l) \sin\left(\frac{4h}{\omega}\right) - \hat{\sigma}_l^z \sin(\hat{\theta}_l) \right\} \right] \exp [-iH_B T] \\ &= \exp \left[-2i \sum_{l,m \in A} J_{lm} \hat{\sigma}_l^y \hat{\sigma}_m^y \frac{T}{2} \right] \exp \left[-i\epsilon_A \pi \sum_{\substack{l,m \in A \\ l \neq m}} J_{lm} \hat{\sigma}_l^z \hat{\sigma}_m^y \frac{T}{2} \right] \exp \left[\frac{i\epsilon_A \pi}{2} \sum_{l \in A} \left\{ \hat{\sigma}_l^x \left(\cos(\hat{\theta}_l) \cos\left(\frac{4h}{\omega}\right) + 1 \right) \right. \right. \\ &\quad \left. \left. + \hat{\sigma}_l^y \cos(\hat{\theta}_l) \sin\left(\frac{4h}{\omega}\right) - \hat{\sigma}_l^z \sin(\hat{\theta}_l) \right\} \right] \exp [-iH_B T]. \quad (\text{B6}) \end{aligned}$$

Next, we apply the Baker-Campbell-Hausdorff formula [37] successively to all pairs of exponents in the RHS, neglecting all operators with norms $\mathcal{O}(T^2)$ as before, followed by substitution into the RHS of Eqn. B2. Finally, substitution into Eqn. B1 yields the effective Floquet Hamiltonian in the high-frequency limit,

$$\begin{aligned} H^{\text{eff}} &\approx \frac{\hbar}{2} \sum_{l,m \in A} J_{lm} \hat{\sigma}_l^y \hat{\sigma}_m^y + \frac{\hbar \epsilon_A \pi}{4} \sum_{\substack{l,m \in A \\ l \neq m}} J_{lm} \hat{\sigma}_l^z \hat{\sigma}_m^y + \frac{\hbar}{2} \sum_{l,m \in B} J_{lm} \hat{\sigma}_l^y \hat{\sigma}_m^y + \frac{h\hbar}{\pi} \sum_{m \in B} \hat{\sigma}_m^z \\ &\quad - \frac{\hbar \pi \epsilon_A}{4T} \sum_{l \in A} \left\{ \hat{\sigma}_l^x \left[\cos(\hat{\theta}_l) \cos\left(\frac{4h}{\omega}\right) + 1 \right] + \hat{\sigma}_l^y \cos(\hat{\theta}_l) \sin\left(\frac{4h}{\omega}\right) - \hat{\sigma}_l^z \sin(\hat{\theta}_l) \right\}. \quad (\text{B7}) \end{aligned}$$

In the limit of very high frequencies, $T \rightarrow 0$, leading to asymptotically vanishing $\hat{\theta}_l$. In this limit, the coupling between regions manifests as effective fields $\sim \hat{\sigma}_l^{x,y}$ in region A whose intensities depend only on ϵ_A , and the ratio $\frac{4h}{\omega}$. When h is set to an odd multiple of $\pi\omega/4$, these effective fields vanish in the asymptotic limit, causing the regions A and B to decouple completely.